Nuclear Engineering and Technology 54 (2022) 2625–2634

Contents lists available at ScienceDirect

Nuclear Engineering and Technology

journal homepage: www.elsevier.com/locate/net

Original Article

Goal-oriented multi-collision source algorithm for discrete ordinates transport calculation

Wang Xinyu, Zhang Bin*, Chen Yixue

School of Nuclear Science and Engineering, North China Electric Power University, Beijing, 102206, China

ARTICLE INFO

Article history:
Received 15 November 2021
Received in revised form
18 January 2022
Accepted 19 January 2022
Available online 23 January 2022

Keywords:
Radiation transport
Discrete ordinates method
Multi-collision source
Goal-oriented

ABSTRACT

Discretization errors are extremely challenging conundrums of discrete ordinates calculations for radiation transport problems with void regions. In previous work, we have presented a multi-collision source method (MCS) to overcome discretization errors, but the efficiency needs to be improved. This paper proposes a goal-oriented algorithm for the MCS method to adaptively determine the partitioning of the geometry and dynamically change the angular quadrature in remaining iterations. The importance factor based on the adjoint transport calculation obtains the response function to get a problem-dependent, goal-oriented spatial decomposition. The difference in the scalar fluxes from one high-order quadrature set to a lower one provides the error estimation as a driving force behind the dynamic quadrature. The goal-oriented algorithm allows optimizing by using ray-tracing technology or high-order quadrature sets in the first few iterations and arranging the integration order of the remaining iterations from high to low. The algorithm has been implemented in the 3D transport code ARES and was tested on the Kobayashi benchmarks. The numerical results show a reduction in computation time on these problems for the same desired level of accuracy as compared to the standard ARES code, and it has clear advantages over the traditional MCS method in solving radiation transport problems with reflective boundary conditions.

© 2022 Korean Nuclear Society, Published by Elsevier Korea LLC. This is an open access article under the CC BY-NC-ND license (http://creativecommons.org/licenses/by-nc-nd/4.0/).

1. Introduction

Radiation transport calculation is essential for designing and evaluating nuclear devices such as particle accelerators, medical radiation treatments and nuclear reactors. The discrete ordinates method (S_N) is one of the primary methods for solving the linear Boltzmann equation and has been used in many radiation transport codes [1]. In the S_N calculation, the approximation of the angular variables inevitably leads to discretization errors. Especially for problems with void regions such as large cavities and long ducts, the strong anisotropic distribution of angular flux is exceptionally prone to cause ray effects, resulting in non-physical oscillations in flux distribution [2]. Since the quadrature sets are not arbitrarily rotation invariant, the angular discretization error is an inherent defect of the S_N method. This shortcoming seriously affects the reliability of the S_N calculation, and its mitigation technology has always been one of the research hotspots in this field. It's worth noting that the heterogeneous effect of the angular flux is a process of gradual weakening with iteration. Traditionally, the flux from every iteration is combined, with the same quadrature applied to the combined flux, but in fact, the quadrature requirements generally decrease with each iteration. In other words, different quadrature sets can be used for each iteration, and an intelligent scheme can be developed to choose, on the fly, an appropriate angular quadrature for each iteration.

Several methods have been proposed for mitigating the angular discretization error. The first is local angular refinement. It increases the discrete directions of the quadrature sets in a region with angular flux anisotropy to improve the numerical integration precision. Longoni investigated ordinate splitting (OS) [3]and regional angle refinement (RAR) [4]. OS and RAR are effective for transport problems with strong angular correlation, but the direction of refinement should be selected in advance according to the calculation model. In 2021, Dai studied an adaptive algorithm based on linear discontinuous finite element quadrature sets over an icosahedron, generating a problem-dependent local refinement quadrature set [5]. Although local angular refinement can effectively mitigate the angular discretization error, it is difficult to generate sufficient directions at a reasonable computational cost

* Corresponding author.
E-mail address: zhangbin@ncepu.edu.cn (Z. Bin).

https://doi.org/10.1016/j.net.2022.01.020
1738-5733/© 2022 Korean Nuclear Society, Published by Elsevier Korea LLC. This is an open access article under the CC BY-NC-ND license (http://creativecommons.org/licenses/by-nc-nd/4.0/).

when the source region is far from the target. Stone first studied the angular adaptive method in 2007 [6]. He developed the adaptive quadrature schemes in two dimensions based on standard quadrature sets. On this basis, Jarrell and Lau extended the algorithm to three-dimensional by using linear discontinuous finite element (LDFE) quadrature sets and developed an optimal mapping algorithm [7,8]. In 2018, with the spherical quadrilateral quadrature sets, Zhang evaluated a goal-oriented angular adaptive algorithm based on the adjoint value theory to mitigate ray effects [9]. However, the accuracy of the applied quadrature sets may hinder the development of this angular adaptive method. The collision source method is another widely used in discretization errors mitigation. The collision source method calculates the uncollided and collided fluxes using a high-order transport or analytical method. In 1989, Alcouffe modified the standard first-collision source (FCS) method using the angle-integrated mesh-cell balance equation to improve the calculation accuracy [10]. In 1993, Winarno used the n'th collision source method within the FCS framework to mitigate ray effects in calculating multidimensional photon transport but only dealt with the one-group energy problem of isotropic scattering [11]. In 2015, Walters developed the adaptive collision source method, obtaining the flux from each scattering source iteration with a potentially different quadrature order [12].

In previous studies, we developed the multi-collision source (MCS) method, which builds off the FCS method by separating the uncollided and collided fluxes [13]. The MCS method calculates multi-collision sources via spatial decomposition to solve the S_N equation for serious anisotropy problems and extends the ability to eliminate ray effects to secondary ray effects and numerical diffusion. Unfortunately, besides limitations of the algorithm in terms of boundary conditions, computational efficiency, the selection of ray tracing region in the MCS method relies on user intuition or prior knowledge of specific issues. The above problems restrict the usage scenario of the method.

The goal-oriented MCS method is composed of both goal-oriented spatial decomposition and dynamic quadrature. It can achieve good speedups and more robust to a wide variety of problems for which the MCS is not as influential. The rest of the paper is organized as follows. An overview of our algorithm is presented in Section II. Results are presented in Section III, and conclusions and further work are summarized in Section IV.

2. Methodology

2.1. Multi-collision source algorithm

One-group steady-state neutron transport equation can be written in operator form as

$$\boldsymbol{L}\Psi = \boldsymbol{S}\Psi + Q \tag{1}$$

where Ψ is the angular flux, Q is the localized source, the streaming-collision operator $\boldsymbol{L}$ and scattering operator $\boldsymbol{S}$ are defined as

$$\boldsymbol{L} = \boldsymbol{\Omega}\cdot\nabla + \Sigma_t \tag{2}$$

$$\boldsymbol{S} = \int_0^\infty dE' \int_{4\pi} \Sigma_s d\Omega \tag{3}$$

where Σ_t is the macroscopic total cross-section and Σ_s is the macroscopic scattering cross-section.

The general source iteration scheme is

$$\boldsymbol{L}\Psi^{(l+1)} = \boldsymbol{S}\Psi^{(l)} + Q \tag{4}$$

where $\psi^{(l)}$ is the flux after iteration l. For problems with scattering, if the initial scattering source is estimated to be zero ($\psi^{(0)} = 0$), the source iteration angular flux estimate after l sweeps is, physically, the angular flux due to particles that have experienced at most l-1 scattering events. After a sufficient number of iterations, both sides of the equation will converge to within some given tolerance.

In the MCS method, we expand the total flux into the fluxes from different collision sources. Then, solving (1) is formally equivalent to solving the following system of equations

$$\begin{aligned} &\boldsymbol{L}\Psi^{(0)} = Q \\ &\boldsymbol{L}\Psi^{(1)} = \boldsymbol{S}\Psi^{(0)} \\ &\cdots \\ &\boldsymbol{L}\Psi^{(l)} = \boldsymbol{S}\Psi^{(l-1)} \qquad (l \geq 1) \end{aligned} \tag{5a}$$

and

$$\begin{aligned} &\boldsymbol{L}\Psi^{(l+1)} = \boldsymbol{S}\Psi^{(l)} \\ &\boldsymbol{L}\left(\Psi^{(l+1)} + \Psi^{(l+2)}\right) = \boldsymbol{S}\left(\Psi^{(l)} + \Psi^{(l+1)}\right) \\ &\cdots \\ &\boldsymbol{L}\left(\Psi^{(l+1)} + \cdots + \Psi^{(n)}\right) = \boldsymbol{S}\left(\Psi^{(l)} + \cdots + \Psi^{(n-1)}\right) \qquad (n \to \infty) \end{aligned} \tag{5b}$$

For iteration l, the method splits the angular flux into semi-analytical and S_N parts. In order to calculate these two parts, the method divides the spatial domain into two hypothetical parts, regions A and B, and the fixed-source is always in region A. The scattering source ($\boldsymbol{S}\psi^{(l-1)}$) takes the form of region A (Q_A) and region B (Q_B), where $\boldsymbol{S}\psi^{(l-1)} = Q_A + Q_B$. Then we can redefine the scattering source distribution using the spatial position of particle scattering. The angular fluxes that are scattered in regions A and B are now defined as $\boldsymbol{L}^{-1}Q_A$ and $\boldsymbol{L}^{-1}Q_B$. $\boldsymbol{L}^{-1}Q_A$ can be solved semi-analytically using ray tracing

$$\boldsymbol{L}^{-1}Q_A = \delta(\boldsymbol{\Omega} - \boldsymbol{\Omega}_{A\to r}) \frac{\boldsymbol{S}\psi^{(l-1)}}{4\pi} \frac{e^{-\tau(\mathbf{r}_A,\mathbf{r})}}{|\mathbf{r}_A - \mathbf{r}|^2} \tag{6}$$

where $\delta(\boldsymbol{\Omega} - \boldsymbol{\Omega}_{A\to r})$ is the Dirac delta function, $\mathbf{r}_A$ and $\mathbf{r}$ are the locations of the point source and targeting grid, $\tau(\mathbf{r}_A, \mathbf{r})$ is the optical distance between $\mathbf{r}_A$ and $\mathbf{r}$, and $|\mathbf{r}_A - \mathbf{r}|$ is the distance between $\mathbf{r}_A$ and $\mathbf{r}$. $\boldsymbol{L}^{-1}Q_B$ is solved by traditional S_N operation, is commonly referred to as a transport sweep. As mentioned above, the flux after iteration l can be calculated from

$$\psi^{(l)} = \boldsymbol{L}^{-1}Q_A + \boldsymbol{L}^{-1}Q_B \tag{7}$$

and the source term after l'th collision ($Q^{(l)}$) can be written as:

$$Q^{(l)} = \boldsymbol{S}\left(\psi^{(0)} + \ldots + \psi^{(l)}\right) = \boldsymbol{S}\sum_{i=0}^{l}\psi^{(i)} \tag{8}$$

The angular flux after n'th collision (ψ_{SN}) can be solved by traditional S_N transport sweeps. Upon the convergence of the source iterations, the angular flux ψ_{SN} is given by

$$\boldsymbol{L}\left(\sum_{i=l+1}^{n}\psi^{(i)}\right) = \boldsymbol{S}\left(\sum_{i=l+1}^{n}\psi^{(i)}\right) + Q^{(l)} \tag{9}$$

and the total angular flux is given by

$$\psi = \sum_{i=0}^{I} \psi^{(i)} + \psi_{SN} \tag{10}$$

The standard MCS method needs full-scale calculation models (without the reflective boundary conditions) to ensure effectiveness because the ray tracing calculation is difficult to deal with the reflective boundary conditions [14]. A potential downside of the ray tracing in the current implementation is that it is difficult to determine how reflected collided angular flux at the surface affects collided angular flux inside the problem. For the above reasons, the transport sweep with high-order quadrature sets is a substitute for the semi-analytical calculation of the problem with reflective boundary conditions. We illustrate these two treatments in Fig. 1.

2.2. Goal-oriented spatial decomposition

In some radiation transport problems, one is more interested in an accurate detector response than an exact solution across the whole domain. For the previous MCS method, the selection of the MCS region relies on user intuition or prior knowledge of certain issues. The spatial decomposition is related to the physical characteristics of the problem. The goal-oriented algorithm aims to minimize the error in the detector response with as few unknowns as possible. The angular flux in the highest energy group is always the most anisotropic. For multi-group problems, the adjoint transport calculation is only implemented in the highest energy group, and the resulting spatial decomposition scheme is applied to all energy groups.

The monoenergetic forward transport equation is

$$\mathbf{\Omega} \cdot \nabla\psi + \Sigma_t\psi = \int_{\mathbf{\Omega}'} \Sigma_s(\mathbf{\Omega}' \to \mathbf{\Omega})\psi d\mathbf{\Omega}' + Q \tag{11}$$

It is convenient to write in linear operator notation as

$$H\psi = Q \tag{12}$$

and we may define ψ^* as the adjoint function of Ψ. For linear operator H, its adjoint operator H* can be defined as

$$\langle \psi^*, H\psi \rangle = \langle \psi, H^*\psi^* \rangle \tag{13}$$

The neutron importance is expressed by a solution of the adjoint transport equation driven by a source related to detector response, and it obeys the adjoint transport equation

$$-\mathbf{\Omega} \cdot \nabla\psi^* + \Sigma_t\psi^* = \int_{\mathbf{\Omega}'} \Sigma_s(\mathbf{\Omega} \to \mathbf{\Omega}')\psi^* d\mathbf{\Omega}' + Q^* \tag{14}$$

where ψ^* is the adjoint angular flux, Q* is the adjoint source. Again, use operator notation to write (14) as

$$H^*\psi^* = Q^* \tag{15}$$

The differences with the forward transport equation are the sign of the streaming term and different source terms (i.e., the detector cross-section (Σ_d) instead of the external source). The larger the adjoint angular flux is, the larger is the probability that neutrons in that location in phase-space will be detected. The S_N method only solves the transport equation in a limit number of directions, so the adjoint scalar flux is used to estimate the neutron importance in this paper, as in (16)

$$\phi^* = \int_{4\pi} \psi^* d\mathbf{\Omega} \tag{16}$$

Neutron importance mainly focuses on the interesting physical quantity. It shows the relative contribution in different phase spaces for the detector response without the contribution of forward transport solution. We optimize the spatial decomposition scheme based on contributon theory [15]. The angular contributon flux is defined as the product of the forward and adjoint angular fluxes

$$C(\boldsymbol{r}, \mathbf{\Omega}) = \psi(\boldsymbol{r}, \mathbf{\Omega}) \cdot \psi^*(\boldsymbol{r}, \mathbf{\Omega}) \tag{17}$$

Then multiply (11) by ψ^* and (14) by Ψ and subtract to obtain the contributon transport equation

$$\mathbf{\Omega} \cdot \nabla\psi\psi^* = \psi^* \int_{\mathbf{\Omega}'} \Sigma_s(\mathbf{\Omega}' \to \mathbf{\Omega})\psi d\mathbf{\Omega}' - \psi \int_{\mathbf{\Omega}'} \Sigma_s(\mathbf{\Omega} \to \mathbf{\Omega}')\psi^* d\mathbf{\Omega}' + Q\psi^* - Q^*\psi \tag{18}$$

where $C(\boldsymbol{r}, \mathbf{\Omega})$ is a function indicating how the contributions to particles within mesh space $\boldsymbol{r}$ and along direction $\mathbf{\Omega}$. This equation contains contributon cross sections that depend on the adjoint flux associated with the detector. Thus, the importance distribution here depends not only on the source distribution and material properties of the system, but also on the detector used to perceive the response. In this paper, only spatial variables are considered,

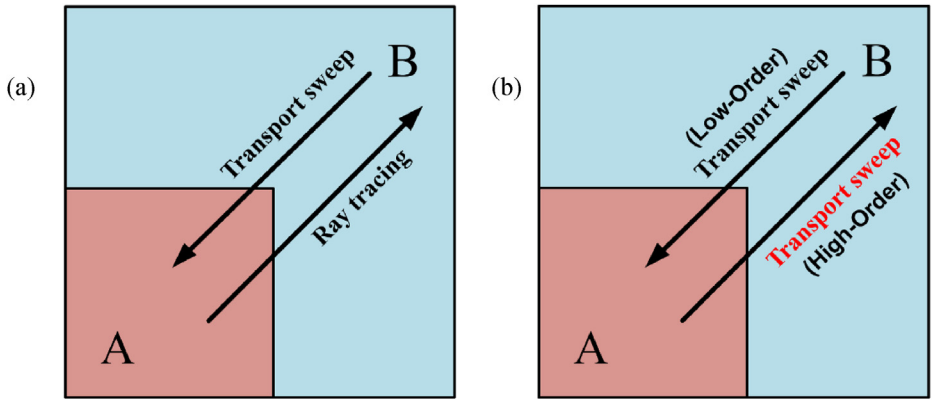

Fig. 1. Sketch of collided flux calculations for the MCS method: (a) semi-analytical calculation, (b) transport sweeps.

and the normalized contribution factor C in the problem domain D is redefined as

$$C(r)=\frac{\phi(r)\cdot\phi^*(r)}{\int_D dr\phi(r)\cdot\phi^*(r)} \tag{19}$$

The contribution factor introduces the forward solution playing the role of the weight coefficient and guides the importance function to be more reasonable in the model. It considers all contributions of forward solution and adjoint solution, which is more suitable than neutron importance as the importance function of spatial decomposition. In the goal-oriented MCS method, the contribution factor acts on the problem domain with two separate parts: the MCS calculation part ($A=\{r|C(r)>\Delta C\}$) and the rest part ($B=D-A$), where ΔC is a user-defined tolerance.

2.3. Dynamic quadrature technique

In the $\psi^{(n)}$ calculation, we use the MCS method for multi-collision sources calculation via spatial decomposition. And in the subsequent iterations, for the calculation of each angular flux, we can use different angular quadrature sets. To achieve this, we need criteria to choose which quadrature set would be most efficient for each iteration. Here, we focus on the two error sources of the error produced by changing the quadrature set in a certain iteration: the relative quadrature error (ε_q) and the relative iterative error (ε_i). The estimated total relative error (E_{tot}) is a combination of the relative iterative and quadrature errors

$$E_{tot}\le\varepsilon_q\cdot\varepsilon_i<\Delta E \tag{20}$$

where ΔE is a user-defined error tolerance for the goal. When changing the quadrature set from order N to N' in a certain iteration, E_{tot} can be calculated as

$$E_{tot}=\frac{\left(\phi^{(0),N}+\cdots+\phi^{(i),N}+\phi^{(i+1),N'}+\cdots+\phi^{(\infty),N'}\right)-\left(\phi^{(0),N}+\cdots+\phi^{(\infty),N}\right)}{\left(\phi^{(0),N}+\cdots+\phi^{(\infty),N}\right)}=\frac{\left(\phi_t^{(i),N}-\phi_t^{(\infty),N}\right)-\left(\phi_t^{(i),N'}-\phi_t^{(\infty),N'}\right)}{\phi_t^{(\infty),N}} \tag{21}$$

where $\phi_t^{(i)}$ is the total scalar flux after i sweeps.

The relative quadrature error (ε_q) due to the quadrature change is one of the error sources of the total relative error. The scattering process tends to distribute the angular flux more evenly over angles, we assume that the relative quadrature error goes down with the number of iterations. To estimate the error of using a new quadrature set, we perform an extra transport sweep with a lower-order quadrature set after completing one iteration and compare the two results. With the current iteration scalar flux ($\phi^{(i),N}$) and the extra calculation scalar flux ($\phi^{(i),N'}$), we can estimate the relative quadrature error:

$$\varepsilon_q^{(i)}=\frac{\phi^{(i),N'}-\phi^{(i),N}}{\phi^{(i),N}}, \tag{22}$$

From (22), the total scalar flux with N'-order quadrature set can be expressed by the following inequality using assumption $\varepsilon_q^{(i+1)}\le\varepsilon_q^{(i)}$

$$\sum_{l=i+1}^{\infty}\phi^{(l),N'}=\sum_{l=i+1}^{\infty}\left(1+\varepsilon_q^{(l)}\right)\phi^{(l),N'}\le\left(1+\varepsilon_q^{(i)}\right)\sum_{l=i+1}^{\infty}\phi^{(l),N} \tag{23}$$

Then, from (21) we obtain

$$E_{tot}\le\varepsilon_q\frac{\phi_t^{(\infty),N}-\phi_t^{(i),N}}{\phi_t^{(\infty),N}} \tag{24}$$

Here, the second factor on the right side of (24) is the second potential error source of the total relative error, which does not depend on the quadrature formula. This error source is defined as the relative iterative error (ε_i)

$$\frac{\phi_t^{(\infty)}-\phi_t^{(i)}}{\phi_t^{(\infty)}}\le\frac{\phi_t^{(\infty)}-\phi_t^{(i)}}{\phi_t^{(i)}}=\varepsilon_i \tag{25}$$

The source iteration of the linear Boltzmann equation exhibits monotonic convergence. The scalar flux in each successive iteration should decay by the spectral radius (σ) after enough iterations. The spectral radius should be less than 1 to ensure source iteration scheme convergence. An equivalent definition, which allows σ to be estimated without knowing the limit of the sequence of iterates, is given as

$$\sigma=\frac{\phi_t^{(n)}-\phi_t^{(n-1)}}{\phi_t^{(n-1)}-\phi_t^{(n-2)}}=\frac{\phi^{(n)}}{\phi^{(n-1)}} \tag{26}$$

When the iteration reaches the convergence criterion, the error between calculation results and exact solution is expressed as follows

$$\phi_t^{(\infty)}-\phi_t^{(n)}\le\frac{\sigma}{1-\sigma}\left(\phi_t^{(n)}-\phi_t^{(n-1)}\right)=\frac{\sigma}{1-\sigma}\phi^{(n)} \tag{27}$$

The relative iterative error estimate can thus be found by inserting (26) and (27) into (25) to give

$$\varepsilon_i=\frac{\sigma}{1-\sigma}\frac{\phi^{(n)}}{\phi_t^{(n)}}=\frac{\phi^{(n)}/\phi^{(n-1)}}{1-\phi^{(n)}/\phi^{(n-1)}}\frac{\phi^{(n)}}{\phi_t^{(n)}} \tag{28}$$

2.4. Implementation

The previous sections have presented the criterion measures suitable for spatial decomposition and dynamic quadrature. This section describes how to use these criteria in the goal-oriented MCS method. The simplest means to present this is in the form of pseudo-code as shown in Algorithm 1 but the algorithm will also be described in the text.

Before the transport solution, the calculation for the forward and

the adjoint fluxes are done separately in the pre-processing stage and used to estimate the contribution factor. The next step is to form a spatial decomposition for MCS calculations based on the contribution factor distribution. Therefore, we do not include the time spent in calculating the contribution factor in the total GM calculation time. The factor definitions are such that the region should be MCS calculation region if the user-defined tolerance ΔC has been met. After MCS calculation (l iterations, as shown in Algorithm 1), additional error estimation is required as the driving force to reduce the quadrature order since the quadrature set with high order may not be necessary in the following iterations. If the estimated error is less than the tolerance ΔE, the quadrature order is lowered.

Algorithm 1. The goal-oriented MCS method with dynamic quadrature.

The problem domain D is divided into nonoverlapping cells D_k, $k = 1, \cdots, K$.

The number of total inner iterations is L.

Do ($n = 1$ to L)

[Solve for angular flux distributions in first l iterations by the MCS method.]

If ($n <= l$) **Then**

[Loop over each spatial grid.]

Do ($D_k = 1$ to K)

If ($C(D_k) > \Delta C$) **Then**

Calculate $\boldsymbol{L}^{-1}Q_A$ with a high-order method.

Else

Update Q_B.

End If

End Do

Calculate $\boldsymbol{L}^{-1}Q_B$.

$\psi^{(n)} = \boldsymbol{L}^{-1}Q_A + \boldsymbol{L}^{-1}Q_B \rightarrow \phi^{(n)}$

[Dynamical quadrature is used in remaining iterations.]

Else If ($n >= l+1$) **Then**

$\psi^{(n)} = \boldsymbol{L}^{-1}\boldsymbol{S}\psi^{(n-1)} \rightarrow \phi^{(n)}$

Calculate $\varepsilon_q^{(n)}$ with N'-order quadrature set and $\varepsilon_i^{(n)}$.

If ($\varepsilon_q^{(n)} \cdot \varepsilon_i^{(n)} < \Delta E$) **Then**

Change the quadrature set from order N to N'.

End If

End If

$\phi_t = \phi_t + \phi^{(n)}$

End Do

3. Results and discussion

The generation of contribution factor, algorithms of calculating the multi-collision source, and model features determine the simulation efficiency and accuracy together. To investigate these effects, this goal-oriented algorithm is applied to three Kobayashi benchmarks [16]. The algorithm has been be implemented into the three-dimensional particle transport code ARES [17] for assessment. Table 1 lists the source strength and cross-section in three cases of Kobayashi benchmarks. As a metric of error, the root mean square of relative errors (E_{RMS}) of the scalar flux was calculated, as compared to the reference results. The E_{RMS} can be calculated as follow:

$$E_{RMS} = \sqrt{\frac{1}{M}\sum_{m=1}^{M}\left(\frac{\phi_m - \phi_{m,ref}}{\phi_{m,ref}}\right)^2} \tag{29}$$

where m is the spatial index, M is the total number of spatial elements, ϕ_m is the calculated scalar flux, and $\phi_{m,ref}$ is the scalar flux of the reference results.

In practical terms, it will be important to compare computation time for a given level of error when comparing methods. Because of the inability of analytical calculation for reflection boundary conditions, vacuum boundary conditions were imposed on all the external boundaries in the standard MCS calculation. But for the goal-oriented MCS calculation, the application of reflective boundary conditions can significantly reduce the number of unknowns, which is eight times difference between the two methods. Six calculation schemes were used for testing and analysis of goal-oriented spatial decomposition and dynamic quadrature technique: the standard S_N method, S_N method with dynamic quadrature (DQ), the goal-oriented MCS method with dynamic quadrature (GM-DQ), the goal-oriented MCS method with full-scale model (GM-full), the standard MCS method with P_NT_N-S_{80} (SM-S_{80}) and the standard MCS method with ray tracing (SM-RT). The first three schemes use 1/8 model with reflective boundary and the last three schemes use full-scale model. For the standard S_N method, the transport equation was solved with P_NT_N-S_{32} or P_NT_N-S_{60}, respectively. For dynamic quadrature, a smooth quadrature sequence including five P_NT_N quadrature sets ($S_8/S_{16}/S_{32}/S_{40}/S_{60}$) was used in the calculation. The manual partitioning of the geometry in the SM scheme is done including the source region and the void region, while the partitioning of the geometry in the GM scheme is goal-oriented based on the contribution factor distribution (defined in (19)). The calculation models of forward and adjoint calculations are same as the transport calculation. P_NT_N −S_{32} is used for these calculations and the spatial discretization scheme uses the Directional Theta Weighted (DTW) with an iterative convergence criterion of 10^{-4}. The number of collisions set by GM and SM was 1, meaning that both methods calculate the uncollided flux and the first-collided flux with a high-order method (ray tracing technology or P_NT_N-S_{80} quadrature set).

3.1. Kobayashi-I benchmark

The Kobayashi-I benchmark is a square shielding block containing a cavity. An isotropic source is in the center of the cavity. This model will allow the testing of the ability of our methods in problems with a cavity. The calculation models of the SM and GM are different, as shown in Fig. 2. The mesh used for the SM calculation was composed of 100 × 100 × 100 Cartesian grids, but it used only 50 × 50 × 50 grids for the GM calculation.

The results of the standard S_N method with different quadrature sets (S_{16}—S_{60}) prove that the maximum relative error locates at the coordinate (95, 95, 95). On this account, the coordinate is defined as the adjoint source region, and the adjoint calculation result is shown in Fig. 3. Fig. 4 shows the contribution factor distribution at different tolerances. For this model, the MCS calculation used a user-defined tolerance ΔC of 1×10^{-5}.

Table 1
Source strengths and cross-sections of Kobayashi benchmarks.

Regions	Source/$n\cdot cm^{-3}\ s^{-1}$	Total Cross Sections/cm^{-1}	Scattering Cross Sections/cm^{-1}
1	1	0.1	0.05
2	0	10^{-4}	0.5×10^{-4}
3	0	0.1	0.05

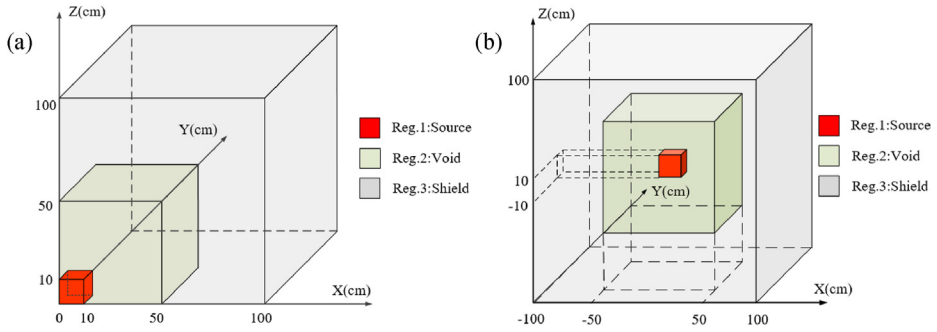

Fig. 2. Geometries of the Kobayashi-I benchmark with different methods. (a) Configuration with the reflective boundary for GM calculation. (b) Configuration of full-scale for SM calculation.

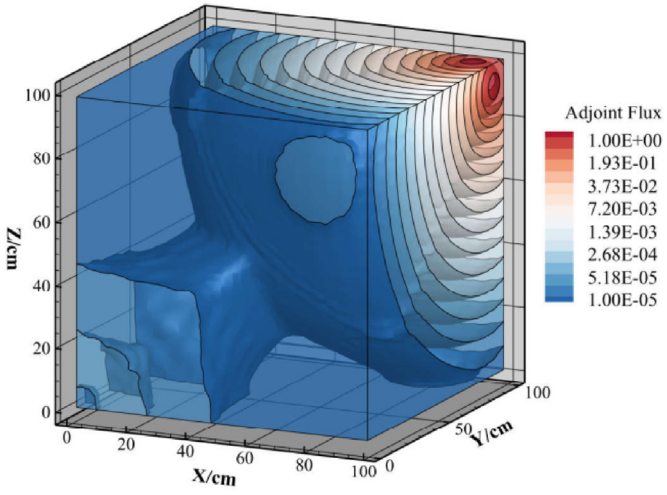

Fig. 3. Adjoint flux distribution for the Kobayashi-I benchmark.

The first issue that needs to be addressed is the balance of the efficiency and accuracy of the dynamic quadrature. The tolerance criterion (ΔE) directly affects the number of quadrature sets used. For a list of quadrature, the more iterations are performed at the high quadrature the more computation time. The calculations were repeated using the dynamic quadrature S_N method for tolerances from 0.5 to 0.001. Results including CPU times and usage of five different quadrature sets are given in Fig. 5. With decreasing, more iterations are performed at the higher quadrature, and the computation time increases. The transition of the quadrature order from high to low appear to fit a pattern that the angular flux becomes extensive and isotropic as the iterations proceed. The results obtained from the preliminary analysis of accuracy and efficiency are shown in Fig. 6. Further analysis showed that all calculations of the dynamic quadrature achieve the same accuracy level as the S_{60} result and show a speedup of between 1.26 and 2.48. As ΔE decreases, the E_{RMS} decreases slightly, while the computation time increases by a significant amount. It is also noted that regardless of chosen parameters (quadrature and tolerance), this method

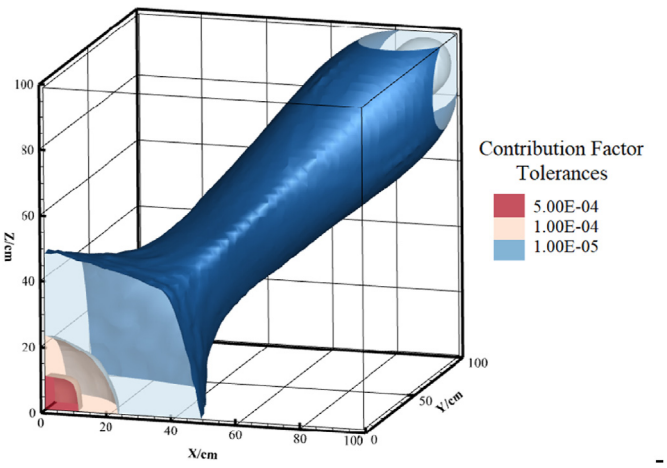

Fig. 4. The contribution factor distribution plots for the Kobayashi-I benchmark at different tolerances.

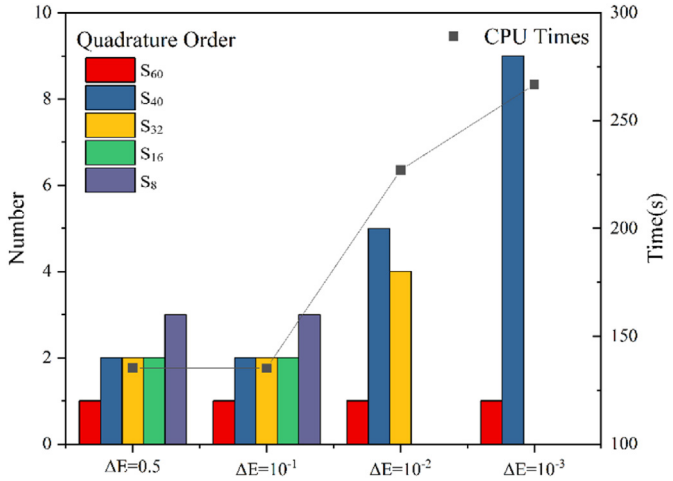

Fig. 5. Effect of the tolerance criterion (ΔE) on the number of times the quadrature used and efficiency for the Kobayashi-I benchmark.

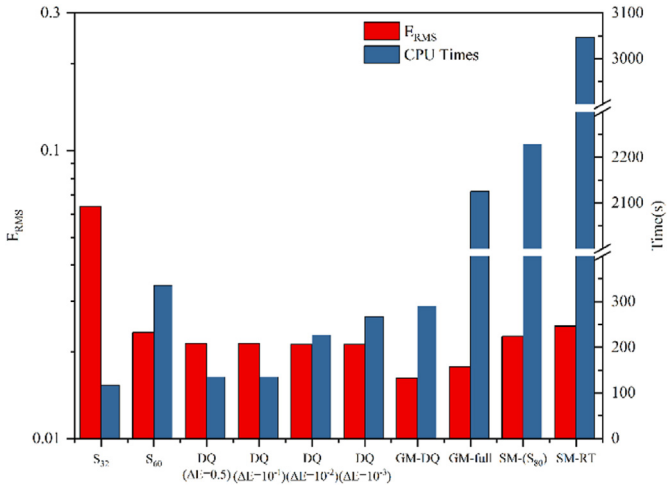

Fig. 6. Comparison of accuracy and efficiency with six calculation schemes for the Kobayashi-I benchmark.

performs better, so a priori knowledge of some optimal parameters is not required to get a speedup.

Fig. 6 also illustrates some of the main characteristics of the MCS methods. Comparing the two results, it can be seen from the data in the figure that the GM-DQ calculation has more efficiency and better precision than the SM-RT calculation. From the efficiency standpoint, this is largely due to two reasons: First, the GM-DQ calculation combines the dynamic quadrature, while the SM-RT calculation does not. The second and most important reason is that the two calculations are under different boundary conditions. For the calculation of collided fluxes, the computational complexity of ray tracing techniques may be higher than that of transport sweeps. In each inner iteration, the calculation amount of transport sweeps is the number of angular discrete directions multiplied by the number of total grids, while the number of rays for ray tracing is

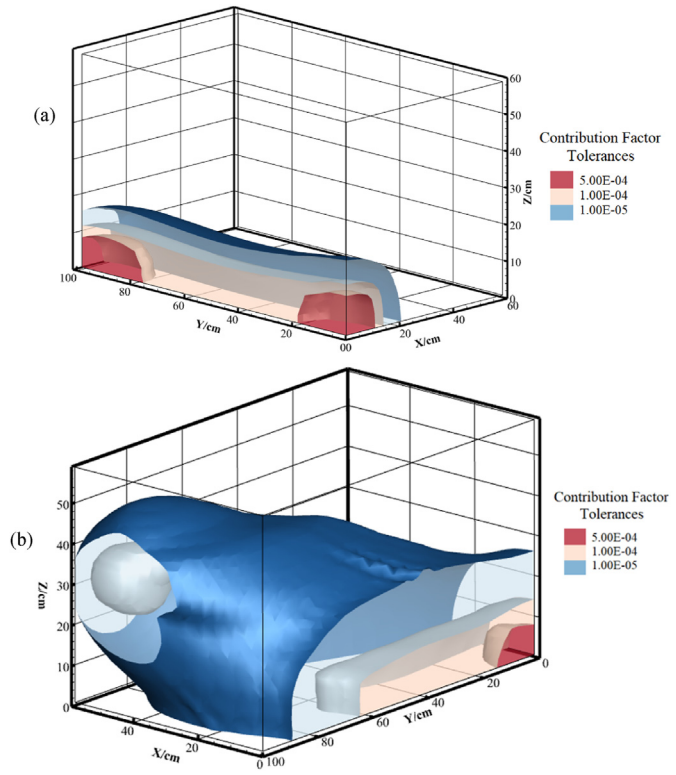

Fig. 9. The contribution factor distribution plots at different tolerances (a) Kobayashi-II benchmark. (b) Kobayashi-III benchmark.

the number of source grids multiplied by the number of total grids. For three-dimensional problems, if the vacuum boundary replaces the reflection boundary, to ensure integrity, the number of grids will be several times more than the original, while the number of angular directions will remain unchanged. In this way, the number

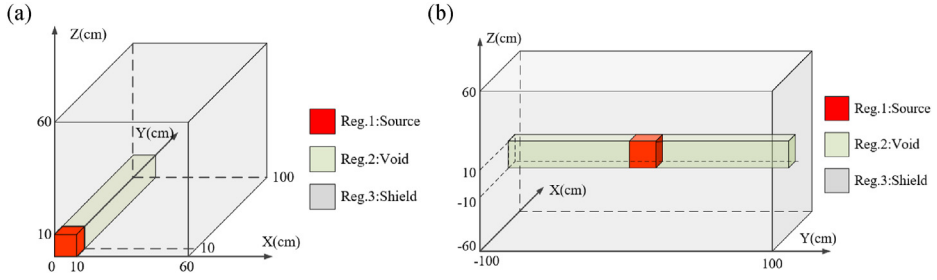

Fig. 7. Geometries of the Kobayashi-II benchmark with different methods. (a) Configuration with the reflective boundary. (b) Configuration of full-scale.

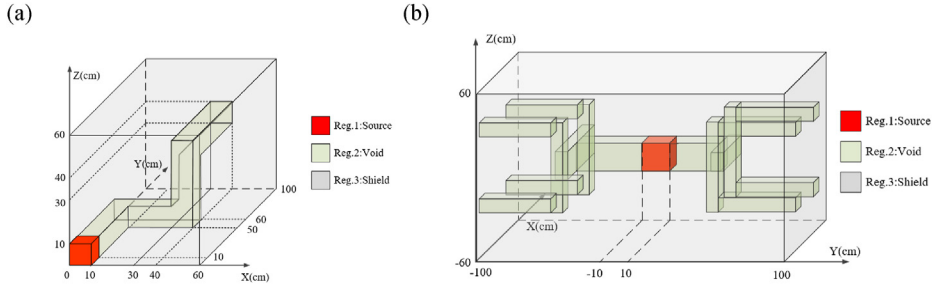

Fig. 8. Geometries of the Kobayashi-III benchmark with different methods. (a) Configuration with the reflective boundary. (b) Configuration of full-scale.

of source grids in MCS calculation is much larger than angular discrete directions, especially for the calculation of collided fluxes. The computation amount of ray tracing is bound to be much larger than that of the higher-order quadrature sets. In the comparison between SM-S_{80} and SM-RT, the efficiency of SM-RT is significant reduced due to its high computation complexity. It should also be noted that the comparison between GM-full and SM-S_{80} indicates that different spatial decomposition schemes may affect the computational efficiency due to the different number of grids in MCS calculation region.

From the standpoint of minimizing the E_{RMS}, this is also due to two reasons: Firstly, the accuracy of transport sweeps depends on the ray effects caused by angular discretization and the numerical diffusion caused by spatial discretization, while that of ray tracing depends on the grid step-size of the source region. The comparison between SM-S_{80} and SM-RT shows the difference between the transport sweeps and ray tracing technique. It should be noted that the numerical diffusion may mutually compensate with the angular discretization error when the mesh is large. Secondly, SM-S_{80} and GM-full have used dissimilar spatial decompositions. The GM-full plan considering all contributions of forward and adjoint solution is better than the original SM one based on model materials.

3.2. Kobayashi-II and Kobayashi-III benchmarks

The Kobayashi-II and Kobayashi-III benchmarks are employed to demonstrate the ability of the GM method in problems with a duct. The Kobayashi II benchmark is a rectangular block made of a half-scattering material containing a straight duct, and the Kobayashi-III differs from Kobayashi-II in that it has a dog-leg duct. The calculation models of the SM and GM are shown in Fig. 7 and Fig. 8. The mesh used for the SM calculation was composed of $60 \times 100 \times 60$ Cartesian grids, but it used only $30 \times 50 \times 30$ grids for the GM calculation.

For Kobayashi-II, because of the straight duct, the angular flux anisotropy increases with distance from the source, and the relative errors of the low-order quadrature sets strongly oscillate non-physically along the duct. The coordinate (5,95,5) is defined as the adjoint source region. The Kobayashi-III is the most difficult Kobayashi problem since particles tend to stream along the dog-leg duct. The duct outlet coordinate (35, 95, 35) is defined as the adjoint source region. Fig. 9 shows the contribution factor distribution at different tolerances. For this model, the MCS calculation used a user-defined tolerance ΔC of 1×10^{-5}, which is the same as that of Kobayashi-I. It is noted that the Kobayashi problems have been addressed to a limited extend with the same user-defined tolerance of 1×10^{-5}, but much more computational experience is needed before the efficacy of current approaches is fully demonstrated.

Fig. 10 provides the CPU times and usage of five different quadrature sets among the four cases of the tolerance criterion for dynamic quadrature. It is apparent from Figs. 5 and 10 that, when $\Delta E = 10^{-1}$, S_{32} quadrature set was called 5 times in the Kobayashi-II benchmark, while it was called only twice in the Kobayashi-I

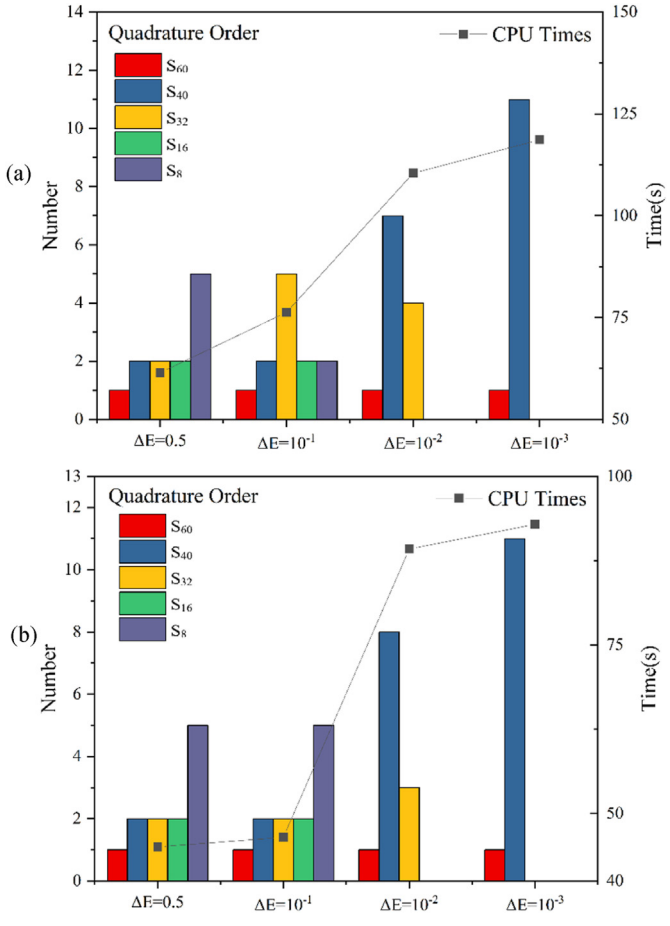

Fig. 10. Effect of the tolerance criterion (ΔE) on the number of times the quadrature used and efficiency. (a) Kobayashi-II benchmark. (b) Kobayashi-III benchmark.

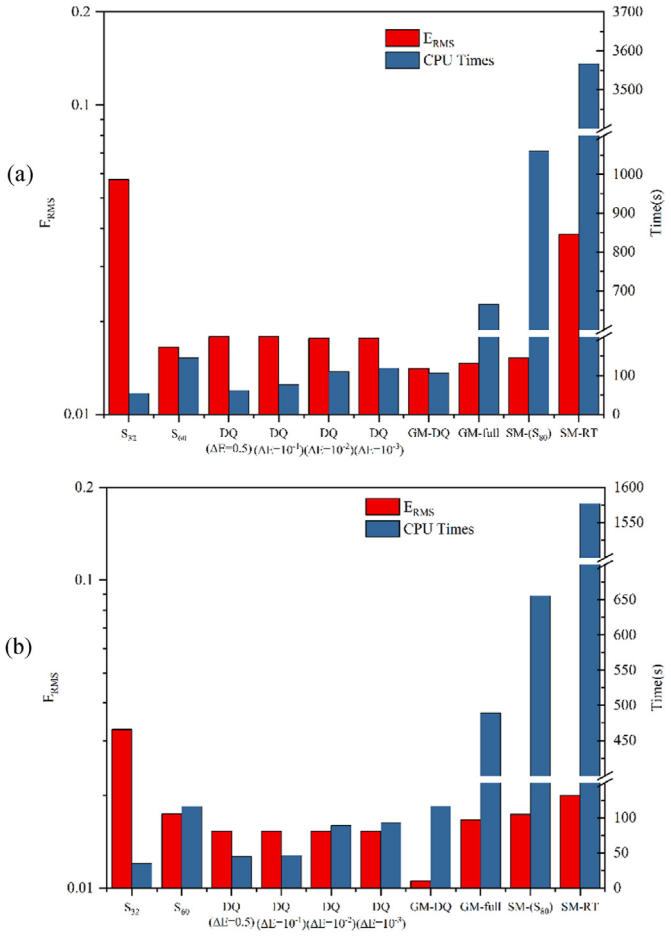

Fig. 11. Comparison of accuracy and efficiency with six calculation schemes. (a) Kobayashi-II benchmark. (b) Kobayashi-III benchmark.

benchmark. It indicates that the number of quadrature set calls is problem-dependent. Several explanations for these results are possible. For radiation transport problems that featured high anisotropy throughout the duct regions, transport sweep requires numerous angular unknowns to achieve the desired accuracy, which means that the quadrature order is difficult to reduce. Even with enough iterations, the algorithm may be still using a high-order quadrature set.

The results obtained from the preliminary analysis of accuracy and efficiency are shown in Fig. 11. The results also indicate that the goal-oriented MCS method outperforms the standard S_N method, S_N method with dynamic quadrature and the standard MCS method for the same desired level of accuracy. For the Kobayashi-II benchmark, the GM-DQ with a time of 106.27s produces an E_{RMS} of 1.41×10^{-2}, whereas the SM-RT with a time of 3566.81s produces an E_{RMS} of 3.82×10^{-2}. Also, for the Kobayashi-III benchmark, the GM-DQ with a time of 116.14s produces an E_{RMS} of 1.05×10^{-2}, whereas the SM-RT with a time of 1577s produces an E_{RMS} of 2.00×10^{-2}. And the speedups arrive at 33.56 and 13.58. The reflection boundary is the main reason for such a huge difference, as analyzed in the Kobayashi- I benchmark above.

The results of the standard S_N method with P_NT_N-S_{60}, SM-RT and GM-DQ schemes are compared with the benchmark solution in Ref. [16], and the relative errors are listed in Tables 2–4. As Table 2 shows, in the source region, the GM-DQ produces a relative error of 0.34%, whereas the SM-RT produces a relative error of 6.25%. However, the maximum relative error of the GM-DQ is about 4.21% at coordinate (75, 75, 75), while the relative error of the SM-RT at

Table 2
Relative errors for the Kobayashi-I Benchmark.

Key Points/cm	P_NT_N-S_{60}	SM-RT	GM-DQ	Key Points/cm	P_NT_N-S_{60}	SM-RT	GM-DQ
	Relative Error				Relative Error		
(5,5,5)	0.37%	6.25%	0.34%	(65,65,65)	−0.02%	−2.06%	−2.14%
(5,15,5)	−0.07%	4.30%	−0.23%	(75,75,75)	−0.88%	−2.61%	−4.21%
(5,25,5)	0.86%	2.78%	0.45%	(85,85,85)	−5.14%	−2.80%	−2.19%
(5,35,5)	0.71%	1.87%	0.93%	(95,95,95)	−7.86%	−1.13%	−3.00%
(5,45,5)	−1.34%	−0.04%	0.77%	(5,55,5)	−3.23%	−1.14%	−0.61%
(5,55,5)	−3.23%	−1.14%	−0.61%	(15,55,5)	−1.69%	0.44%	0.12%
(5,65,5)	−2.56%	0.41%	−1.56%	(25,55,5)	−2.01%	−0.16%	−0.80%
(5,75,5)	−0.16%	0.68%	−1.53%	(35,55,5)	−2.39%	0.46%	−1.71%
(5,85,5)	1.92%	0.98%	−0.37%	(45,55,5)	−2.30%	0.22%	−2.42%
(5,95,5)	3.65%	2.87%	1.99%	(55,55,5)	−1.67%	0.08%	−3.04%
(15,15,15)	−0.19%	0.83%	−0.22%	(65,55,5)	0.03%	0.27%	−1.68%
(25,25,25)	−0.41%	0.98%	−0.37%	(75,55,5)	0.60%	0.96%	−0.70%
(35,35,35)	−0.25%	−0.21%	−0.65%	(85,55,5)	0.83%	1.13%	0.38%
(45,45,45)	−0.05%	1.77%	−0.16%	(95,55,5)	1.40%	2.33%	1.51%
(55,55,55)	1.52%	0.88%	2.48%				

Table 3
Relative errors for the Kobayashi-II Benchmark.

Key Points/cm	P_NT_N-S_{60}	SM-RT	GM-DQ	Key Points/cm	P_NT_N-S_{60}	SM-RT	GM-DQ
	Relative Error				Relative Error		
(5,5,5)	0.37%	3.25%	0.37%	(5,75,5)	−2.58%	1.80%	−2.40%
(5,15,5)	0.58%	1.87%	−0.13%	(5,85,5)	−0.15%	4.02%	−2.25%
(5,25,5)	0.92%	1.97%	0.55%	(5,95,5)	0.90%	5.44%	−1.24%
(5,35,5)	0.63%	2.40%	0.85%	(15,95,5)	1.23%	2.59%	3.12%
(5,45,5)	−0.80%	1.69%	0.38%	(25,95,5)	2.26%	6.70%	1.54%
(5,55,5)	−2.98%	−0.74%	−0.70%	(35,95,5)	1.28%	3.63%	0.06%
(5,65,5)	−3.96%	−0.36%	−1.61%	(45,95,5)	−0.12%	6.14%	−0.93%
				(55,95,5)	0.30%	5.02%	−0.69%

Table 4
Relative errors for the Kobayashi-III Benchmark.

Key Points/cm	P_NT_N-S_{60}	SM-RT	GM-DQ	Key Points/cm	P_NT_N-S_{60}	SM-RT	GM-DQ
	Relative Error				Relative Error		
(5,5,5)	0.35%	2.43%	0.33%	(15,55,5)	0.92%	2.33%	1.95%
(5,15,5)	0.56%	1.49%	−0.19%	(25,55,5)	0.00%	2.39%	0.75%
(5,25,5)	0.90%	1.22%	0.40%	(35,55,5)	0.97%	2.66%	0.34%
(5,35,5)	0.60%	1.09%	0.85%	(45,55,5)	−0.31%	3.43%	0.41%
(5,45,5)	−0.81%	1.02%	0.62%	(55,55,5)	−0.42%	3.81%	0.28%
(5,55,5)	−2.97%	0.90%	−0.44%	(5,95,35)	−2.15%	1.49%	−0.02%
(5,65,5)	−3.40%	0.34%	−1.97%	(15,95,35)	1.49%	1.30%	0.51%
(5,75,5)	−1.32%	0.08%	−2.26%	(25,95,35)	−0.50%	1.07%	0.32%
(5,85,5)	1.00%	0.75%	−1.47%	(35,95,35)	1.56%	2.40%	1.15%
(5,95,5)	1.92%	1.45%	−0.43%	(45,95,35)	0.55%	3.51%	0.24%
(5,55,5)	−2.97%	0.90%	−0.44%	(55,95,35)	4.12%	2.06%	2.21%

the same coordinate is only 2.61%. As can be seen from Table 3, in the source region, the GM-DQ produces a relative error of 0.37%, whereas the SM-RT produces a relative error of 3.25%. However, the maximum relative error of the GM-DQ is about 3.12% at coordinate (15, 95, 5), while the relative error of the SM-RT at the same coordinate is only 2.59%. From Table 4, we can see that the GM-DQ produces a relative error of 0.33% in the source region, whereas the SM-RT produces a relative error of 2.43%. However, the maximum relative error of the GM-DQ is about 2.26% at coordinate (5,75,5), while the relative error of the SM-RT at the same coordinate is only 0.08%. For each benchmark, the scalar flux in the source region is overestimated when the ray tracing technique is used, while the results of transport sweeps are satisfactory. The results reflect the restrictions of the ray tracing technique. The ray tracing calculation is on a straight line between a source point and target mesh center. If the model is divided too coarsely, the flux calculation will produce large errors. On the other hand, the relative errors perform irregular changing with increasing distance from the source due to ray effects, the result of ray tracing is better than that of transport sweeps in the area far away from the source. The advantage of the transport sweep is that it can exactly describe the scalar flux in the source region, and the advantage of ray tracing is to effectively mitigate the ray effects.

4. Conclusions

In this paper, a goal-oriented multi-collision source method was proposed to solve the linear Boltzmann equation, specifically for application to problems containing void regions and ducts. This algorithm uses spatial decomposition based on contribution factor and dynamic quadrature technique to adaptively determine the partitioning of the geometry and dynamically change the angular quadrature order in the remaining iterations. Numerical results through detailed quantitative analysis indicate that both computation accuracy and efficiency are taken in account for the goal-oriented multi-collision source method compared with the standard MCS method. In Kobayashi problems with cavities and straight ducts, the goal-oriented method exhibits the same accuracy with a speedup of approximately 2 compared to the standard S_N calculation, while speedups are more than 10 compared to the standard MCS calculation. The numerical simulations have proved that the proposed method is more accurate and effective than the standard MCS method in solving problems with reflective boundary conditions. Although more comparisons with practical problems are necessary before the efficiency of our method is fully demonstrated, the results presented here are illuminating. It should be noted that transport sweep with high-order quadrature sets cannot mitigate the ray effects far away from the source. Additionally, for the dynamic quadrature technique, the way of the quadrature error based on scalar fluxes is inefficient. Future studies will focus on the parallel strategy and extend the goal-oriented multi-collision source method to multiple sets of complex radiation transport problems.

Declaration of competing interest

The authors declare that they have no known competing financial interests or personal relationships that could have appeared to influence the work reported in this paper.

Acknowledgements

This work was supported by the National Natural Science Foundation of China (11975097).

References

[1] E.E. Lewis, W.F. Miller, Computational Methods of Neutron Transport, John Wiley & Sons Inc, New Jersey, 1984.
[2] K.D. Lathrop, Remedies for ray effects, Nucl. Sci. Eng. 45 (3) (1971) 255–268.
[3] G. Longoni, A. Haghighat, Development of New Quadrature Sets with the 'Ordinate Splitting' Technique, Salt Lake City, USA, in: ANS International Meeting on Mathematical Methods for Nuclear Applications, 2001.
[4] G. Longoni, A. Haghighat, Development and application of the regional angular refinement technique and its application to non-conventional problems, Seoul, Korea, in: Proceedings of PHYSOR 2002 ANS Topical Meeting, 2002.
[5] N. Dai, B. Zhang, Y.X. Chen, et al., Adaptive discontinuous finite element quadrature sets over an icosahedron for discrete ordinates method, Nucl. Sci. Tech. 32 (2021) 98.
[6] J.C. Stone, Adaptive Discrete-Ordinates Algorithms and Strategies, Texas A&M University, Texas, 2007.
[7] J.J. Jarrell, An Adaptive Angular Discretization Method for Neutral-Particle Transport in Three-Dimensional Geometries, Texas A&M University, Texas, 2010.
[8] C.Y. Lau, Adaptive Discrete-Ordinates Quadratures Based on Discontinuous Finite Elements over Spherical Quadrilaterals, Texas A&M University, Texas, 2016.
[9] B. Zhang, L. Zhang, C. Liu, et al., Goal-oriented regional angular adaptive algorithm for the S_N equations, Nucl. Sci. Eng. 189 (2) (2018) 120–134.
[10] R.E. Alcouffe, R.D. O'Dell, F.W. Brinkley, A first-collision source method that satisfies discrete S_N transport balance, Nucl. Sci. Eng. 105 (2) (1990) 198–203.
[11] E.Y. Winarno, Semi-analytical Partial N'th Collision Source Correction for Multi-Dimensional S_N Photon Transport Calculations, The University of Arizona, Tucson, 1993.
[12] W.J. Walters, Development of the Adaptive Collision Source Method for Discrete Ordinates Radiation Transport, Virginia Polytechnic Institute and State University, Blacksburg, 2015.
[13] X.Y. Wang, B. Zhang, N. Dai, et al., Multicollision source method for discrete ordinates neutron transport calculation, Ann. Nucl. Energy 156 (2021) 108216.
[14] J.W. Kim, Y.O. Lee, Aetius solutions for Kobayashi 3D benchmarks with the first collision source method on the volume source and unstructured tetrahedral mesh, Ann. Nucl. Energy 113 (2018) 446–469.
[15] M.L. Williams, Generalized contributon respons theory, Nucl. Sci. Eng. 108 (1991) 355–383.
[16] K. Kobayashi, N. Sugimura, Y. Nagaya, 3D radiation transport benchmark problems and results for simple geometries with void region, Prog. Nucl. Energy 39 (2) (2001) 119–144.
[17] Y.X. Chen, B. Zhang, L. Zhang, et al., ARES: a parallel discrete ordinates transport code for radiation shielding applications and reactor physics analysis, Sci. Technol. Nucl. Install. (2017) 1–11, 2596727, 2017.